Validation of a sectional soot model based on a constant pressure tabulated chemistry approach for PM, PN and PSDF estimation in a GDI research engine

Cite as: AIP Conference Proceedings **2191**, 020064 (2019); https://doi.org/10.1063/1.5138797
Published Online: 17 December 2019

Marco Del Pecchia, Simone Sparacino, Sebastiano Breda, and Giuseppe Cantore

Validation of a Sectional Soot Model Based on a Constant Pressure Tabulated Chemistry Approach for PM, PN and PSDF Estimation in a GDI Research Engine

Marco Del Pecchia [1, a)], Simone Sparacino [1], Sebastiano Breda [2], Giuseppe Cantore [1]

[1)] Department of Engineering "Enzo Ferrari", University of Modena and Reggio Emilia, Via Vivarelli 10, Modena 41125, Italy
[2)] R&D CFD S.R.L., Via Vivarelli 2, Modena 41125, Italy

[a)]Corresponding author: marco.delpecchia@unimore.it

Abstract. Findings from the International Agency for Research on Cancer (IARC) classified particulate matter (PM) as carcinogenic to humans. While being a promising solution to reduce greenhouse gases (GHG) emissions and increase engine fuel economy, Gasoline Direct Injected (GDI) engines produce a number of particles (PN) of fine size higher than Port Fuel Injected (PFI) ones. As a consequence, the EU commission significantly tightened the emission standards for passenger cars, following which all gasoline engines will have to meet the euro-6d regulation coming into force in 2020. Efforts are made by the research community to understand the root causes leading to soot formation and possibly identify technical solutions to lower it. An important piece of the puzzle is the investigation of soot formation via 3D-CFD. To this aim, relevant efforts have been and are still being paid to adapt soot emissions models, originally developed for Diesel combustion, for GDI units. Among the many available models, one of the most advanced is the so-called Sectional Method. So far, studies presented in literature were not able to formulate a methodology to quantitatively match experimental PM, PN and PSDF without a dedicated soot model tuning. In the present work, a Sectional Method-based methodology to quantitatively predict GDI soot is presented and validated against PM, PN and PSDF measurements on a optically accessible GDI research unit. While adapting the model to GDI soot, attention is devoted to the modelling of soot precursor chemistry: a customized version of a pre-existing chemical kinetics mechanism, used to predict the formation of the key PAH (Polycyclic Aromatic Hydrocarbons) species, is presented and validated via 1D numerical simulations on a premixed flat flame burner dataset available in literature. The present work demonstrates that a Sectional Method-based approach can be a powerful tool to quantitatively predict engine-out soot emissions.

INTRODUCTION

In the last decades, the impact of petrol-powered vehicles on the air quality of the major European cities was demonstrated by several studies. A study [1] presented by the Joint Research Centre (JRC), of the European Commission's science and knowledge service, quantifies in 14% the average road transportation's contribution to PM2.5 emissions in 150 urban areas. The same data increases up to a maximum of 39%, when largest European capitals are considered. These data are of great concern considering that the International Agency for Research on Cancer (IARC), part of the World Health Organization (WHO), classified diesel engine exhaust as carcinogenic to humans [2]. A further study [3], presented by the WHO, concluded that a reduction in exposure to ultrafine particles and other combustion-related products should lead to a reduction in the health effects associated with PM. In order to understand the importance of this problem, in [4] it is reported that urban air pollution is the cause of nearly four million deaths annually. For such reasons, particulate matter (PM), with a detailed focus on particulate number (PN), has been extensively studied in research institutes and in the automotive industry. In several studies [5-7] GDI is reported to emit higher concentration of PM compared to PFI engines. The major concern related to GDI technology is the higher number of ultrafine particles, which is even higher than those of Diesel engines equipped with Diesel Particulate Filter (DPF) [8]. With the aim of reducing the soot engine-out emissions, the EU introduced the euro6 regulations. In particular, from the euro6c stage, entered into force on September 2017, GDI units must meet the 4.5 mg/km and 6.0 $\times 10^{11}$ mg/km, for PM and PN respectively [9]. Such limits represent a non-trivial challenge for engine manufacturers. Several studies focused on the mechanisms leading to soot formation in modern GDI units and it is commonly accepted that direct injection in the combustion chamber can induce incomplete evaporation, liquid fuel impingement on the piston crown and the cylinder liner causing the formation of rich mixture pockets, which constitute preferential area for fuel pyrolysis and soot formation [10]. Therefore, a particular care is mandatory when calibrating modern GDI units to meet the regulations [11]. While providing useful information on the overall

74th ATI National Congress
AIP Conf. Proc. 2191, 020064-1–020064-12; https://doi.org/10.1063/1.5138797
Published by AIP Publishing. 978-0-7354-1938-4/$30.00

engine behavior, experiments can explain the reason leading to soot formation up to a limited extent. For this reason, 3D-CFD simulations have become a powerful tool to give a further insight into soot formation in GDI units [12]. Various modelling approaches have been used in the 3D CFD framework to predict soot emissions. Among these, the sectional method model [13-15] constitutes one of the most advanced mathematical formulation to predict PM, PN, and Particle Size Distribution Function (PSDF) in combustion systems. The model was successfully applied in the RANS framework to predict soot emissions in Diesel engine cases [16-20]. To the extent of the authors' best knowledge, only one study present in literature [21] focused on the application of the sectional method model to predict GDI soot. In such study the authors report a reasonable agreement between 3D-CFD results and experiments in terms of PM and PN of a GDI engine operated at two different operating conditions, while no data were provided for PSDF. In the conclusions, the authors claim that the model, as it is, requires specific tuning when used on different operating points for GDI applications. In the present study, a customized version of the sectional method model is validated against experimental measurements carried out on optically accessible single cylinder research GDI engine at the Istituto Motori of the National Research Council (IM-CNR). The soot experimental dataset was extensively presented in [10], and includes PM, PN and PSDF for a full-load operating condition. In particular, PM and PN data are provided for the overall particle count and for the ultrafine particles, identified as the particle whose diameter is within the $30\ nm \leq d \leq 50\ nm$ range. The specifications of the research engine and further details on the selected operating condition are reported in Table 1. As reported in Table 1, the experimental dataset was collected for a 2000 rpm full-load operating condition. The engine features a commercial cylinder head of an engine with four valves per cylinder, wall-guided direct injection and centrally located spark plug. The power unit is provided with a fused silica window fixed on the piston crown to provide access to the combustion chamber. In the present study the analysis is focused on an early injection strategy. Fuel was delivered in the combustion chamber thanks to a single pulse injection and start of injection was fixed at 340 CAD bTDC. Commercial RON95 gasoline was used as a reference fuel and stoichiometric air-fuel ratio (AFR) strategy was adopted. Regarding exhaust measurements, AFR was monitored with an accuracy of $\pm 1\%$ through measurements with a wide band oxygen gas sensor fitted at the exhaust. During the experiments, particle number and size distributions were measured by means of a TSI Engine Exhaust Particle Sizer 3090 (EEPS) through the electrical mobility methods. The EEPS measured particle size ranging from 5.6 to 560 nm, with a sizing resolution of 32 channels, and provides results with an output frequency of 10 Hz. In the next paragraphs, a suitable fuel model, to generate soot chemistry-based libraries to be used in engine simulations, will be discussed. The 3D-CFD modelling approach will then be described with the specific purpose of highlighting the strategies adopted to retain the highest possible degree of accuracy on soot formation and related processes. To conclude, a quantitative comparison between the predicted soot quantities and the experimental data will be presented.

Displacement	Stroke	Bore	Compression ratio	Number of valves	Revving speed	SOI	EVO	EVC	IVO	IVC
399 cm^3	81.3 mm	79 mm	10:1	4	2000 rpm	340 CAD bTDC	153 CAD bTDC	360 CAD aTDC	363 CAD bTDC	144 CAD bTDC

TABLE 1. Engine specifications and operating condition's details.

FUEL MODEL VALIDATION AND SOOT LIBRARY GENERATION

A wide variety of researches present in literature focused on the mechanisms leading to soot formation. Nevertheless, a certain degree of uncertainty is still present on the hierarchy of the complex interplay between the many factors involved during the combustion process. Although some of the underlying processes are not well-established, it is commonly recognized that soot formation is influenced by both chemical and physical factors [22]. Particle inception, or Nucleation, is the chemistry-based process responsible for the formation of a solid phase from gas phase species, commonly known as Poly-Aromatic Hydrocarbons (PAH). Condensation is another chemistry-driven process by which gas phase soot precursors coagulate onto already existing soot particles. Once a solid phase is formed, particles can collide generating larger soot particles via Coagulation, which is a key physical process. In this chain, surface reaction-based processes, namely Surface Growth and Oxidation, may take place at any stage leading, respectively, to mass addition or mass abstraction from already existing soot particles. As many others soot models, the sectional method relies on detailed chemistry calculations to predict quantitatively the chemistry-based processes involved in soot formation, therefore Nucleation, Condensation, Surface Growth and Oxidation. In this work, a chemistry-based tabulated approach is used to predict soot chemistry-driven processes using zero-dimensional constant pressure reactors on a wide range of engine-relevant thermodynamic and mixture quality conditions. This kind of approach is particularly

suitable to describe mainly premixed sooting flames. For this reason, the approach, coupled with the sectional method, was chosen to estimate soot formation in GDI applications. While being dependent on the combustion characteristics, a fuel's sooting tendency is also dependent on its chemical composition. Therefore, a fuel surrogate matching the gasoline main hydrocarbon constituents is essential to quantitatively estimate soot formation. The sectional method relies on the steady-state assumption between the soot precursors formation in the gas phase and their consumption by nucleation and condensation processes. Therefore, it is straightforward to understand the importance of modelling, with the highest degree of accuracy, all the chemistry-based processes involved in soot formation. For this reason, the so-called PAN chemical kinetics mechanism proposed in [23] to estimate soot precursors formation in GDI applications is used as a basis, in the present study, to estimate the sectional method coefficients for a set of engine-relevant conditions via constant pressure reactors calculations. The PAN mechanism is modified here on purpose to include all the chemical species and reactions needed to estimate the coefficients, as required by the sectional method model. In particular, as reported in [20] the pyrenyl radical A3R5$^-$ ($C_{16}H_9$) is required to estimate the rate of formation of soot precursors in the gas phase $RPAH$. The original PAN mechanism accounts for 85species and 439 reactions and features dedicated sub-mechanism for isooctane, n-heptane and toluene oxidation pathways together with a dedicated PAH sub-mechanism for soot precursors. The PAH sub-mechanism is therefore modified to introduce pyrenyl radical ($C_{16}H_9$) and its main formation/consumption pathways. In particular, the species and the reactions introduced to account for A3R5 and A3R5$^-$ are reported in red, while the species and the reactions represented in green are introduced to close the pathways related to the secondary species involved in A3R5 and A3R5$^-$formation and consumption. The final mechanism, herein referred to as PAN-HY, accounts for 95 species and 489 reactions. In order to validate the modified mechanism, a stabilized burner premixed flame experimental dataset presented in [24] by Inal and Senkan is used as a reference to perform 1D simulations using DARSv4.30 chemistry solver, licensed by SIEMENS PLM. In the experiments, the micro-structure of laminar premixed, atmospheric pressure, fuel-rich flames of n-heptane/oxygen/argon were studied at two reference equivalence ratios. In the present study, the so-called "Flame A" dataset is considered for validation purposes and the related details are summarized in Table 2.

	Cold flow initial velocity [cm/s]	Burner's surface temperature [K]	Equivalence Ratio [-]	Fuel (*n-Heptane*) [%mol]	Oxidizer (O_2) [%mol]	Inert Gas (Ar) [%mol]
Flame A	5.25	700	1.97	5.33	29.70	64.97

TABLE 2. Flame A dataset: flame characteristics and pre-combustion compositions.

A comparison between the interpolated and measured flame temperature profiles is reported in Fig. 1a. For the sake of completeness, a comparison between the computed flame velocity and the measured velocity at the burner's surface is reported in Fig. 2a. It must be noted that an uncertainty of $\pm$ 0.2 mm is reported in terms of measurements positional accuracy. An additional error of $\pm$ 80 K, due to the use of thermocouples is present for the local temperature measurements. Moreover, it is noteworthy that the sampling probes used to measure species concentration might lead to flame perturbations. As highlighted in [26], these perturbations might cause a mismatch between the measured species concentration and the species concentration predicted by imposing the experimental temperature profile in a numerical simulation. To overcome this problem, the experimental mole fraction profiles are shifted $+$ 0.5 mm upstream relative to the unperturbed flame temperature profile as suggested in [27]. This is a minor modification to the experimental dataset if compared to solutions presented in literature studies such as [25], where the experimental temperature profile is adjusted to match the fuel and oxidizer consumption. As visible in Fig. 1b, the calculated mole fraction evolution of the main combustion products is in fairly good agreement with the experimental data, despite the minor shift introduced with respect to the original dataset. With the present setup, n-heptane consumption is slightly overestimated and better results could potentially be achieved using the approach suggested in [25]. Focusing on the small hydrocarbon species, which usually constitute the main building blocks for PAH species formation, it is possible to notice how the proposed PAN-HY mechanism is able to predict the evolution of Acetylene (C_2H_2) and Ethylene (C_2H_4) mole fraction profiles although both are quantitatively underestimated. Since a good agreement was found between the calculated and the measured profiles for the main combustion products, a quantitative comparison between calculated and measured main PAH species profiles was carried out to evaluate the capability of the proposed PAN-HY mechanism to predict soot precursors formation in premixed flames, as reported in Fig. 3. Although a wide variety of PAH species were measured in [24], only the key PAH species are here analyzed. Namely: Benzene ($A1$) and Pyrene ($A4$). Monitoring the aforementioned species, is particularly important because most of the soot precursors start growing from incipient Benzene molecules which grow by addition of carbon atoms following H-abstraction C_2H_2-addition (HACA) mechanism. A particular focus is here devoted to the quantitative estimation of Pyrene mole fraction profile, since the sectional method relies on the assumption that nucleation by two Pyrene colliding molecules and quantitatively estimates $RPAH$ based on Pyrenyl radical

$C_{16}H_9$ and Acetylene C_2H_2 concentrations. In order to evaluate the accuracy of the proposed PAN-HY mechanism, the mechanism proposed by Blanquart et al. [25], here called "Stanford mech.", was chosen as reference. While both mechanisms give a reasonable quantitative prediction of $A1$ and $A3$, a better prediction is given by PAN-HY for $A2$ and especially for $A4$. In particular, it is important to underline how the PAN-HY mechanism is able to quantitatively predict the correct order of magnitude of $A4$, which is conversely underestimated of approximately one order of magnitude by Stanford mechanism. From the observation of Figure 2, it is possible to conclude that the proposed mechanism is a suitable candidate to generate the constant pressure soot libraries to be used in 3D-CFD simulations. To conclude the fuel model formulation, a suitable Toluene Reference Fuel (TRF) with the following composition (n-Heptane 0.123%wt / Isooctane 0.483%wt / Toluene 0.394%wt) was specifically generated to match the properties and auto-ignition characteristics of the RON95 commercial gasoline used in the experiments. Attention was devoted in matching the aromatic content of the commercial gasoline since aromatic molecules are more prone to soot formation compared to alkanes, alkenes and alkynes [22]. More details on the composition of the gasoline used in the experiments can be found in [28]. Having defined a reference fuel model, a constant pressure reactor-based library is generated using SIEMENS PLM DARS v4.30 chemistry solver to estimate the sectional method coefficients on a range of engine-relevant (p, T_u, Φ, EGR) conditions listed in Table 3.

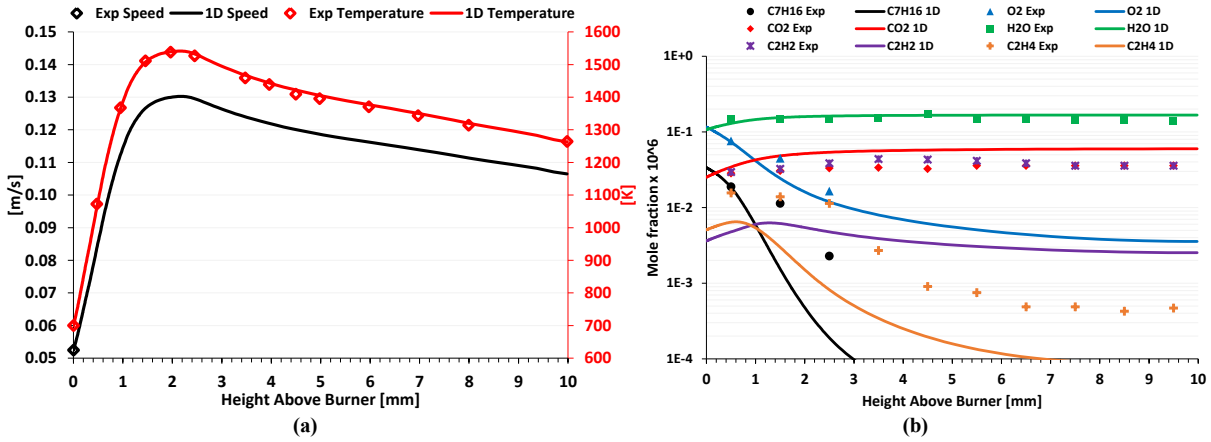

FIGURE 1. (a) Comparison between: experimental (dots)/interpolated (solid line) flame temperature profiles in red, experimental gas velocity measured at the burner's surface and calculated flame speed profile in black. **(b)** Comparison between measured (dots) and calculated species mole fraction (solid line).

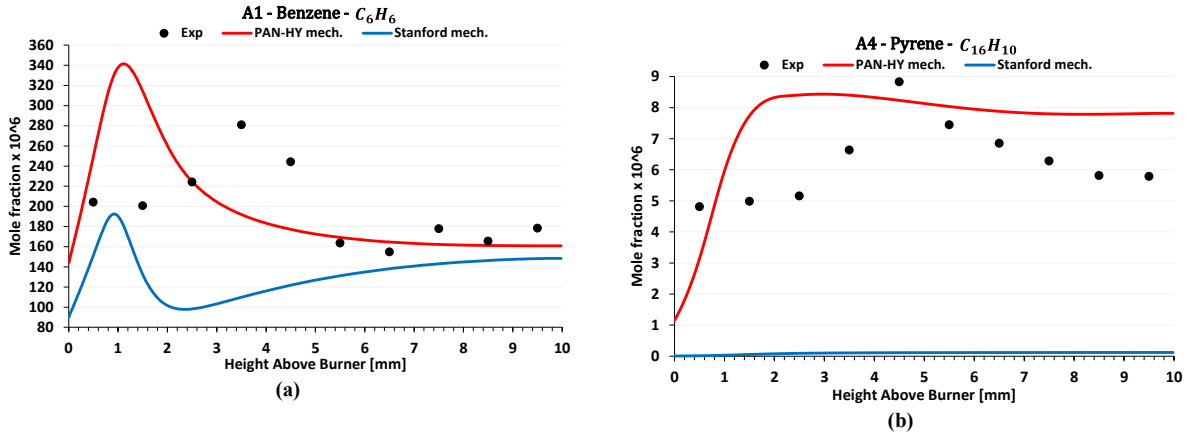

FIGURE 2. Main PAH species mole fraction profiles as a function of HAB: measured (dots), present mechanism PAN-HY (red solid line) and Stanford mechanism [25] (blue solid line) for **(a)** Benzene and **(b)** Pyrene.

As shown in Table 3, a variable stepping strategy was used for equivalence ratio to accurately represent the very high $RPAH$ gradient regions while preserving the cell-to-library access time during run time. Soot coefficients are stored in the library not only as a function of a specific $(p^*, T_u^*, \Phi^*, EGR^*)$ but also based on the value of a progress variable c which tracks the development of the combustion process in the reactor to provide an estimation of the chemistry-based soot formation processes based on a cell-wise combustion development status.

Absolute pressure $\boldsymbol{p}$ $[\boldsymbol{bar}]$	$0.5, 2, 5, 8, 12, 16, 20, 24, 28, 32, 36, 40, 44$
Unburnt temperature $\boldsymbol{T_u}$ $[\boldsymbol{K}]$	$500, 550, 600, 650, 700, 750, 800, 850, 900, 950, 1000$
Equivalence ratio $\boldsymbol{\Phi}$ $[-]$	$0.4{:}\,0.05{:}\,2.0, 2.0{:}\,0.1{:}\,4.0, 4.0{:}\,0.2{:}\,6.0$
EGR [%]	$0, 5, 10, 20, 30, 40, 50, 60$
Progress Variable c $[-]$	$0{:}\,0.01{:}\,1.0$

TABLE 3. Constant pressure-based soot library range and stepping for a selection of engine-relevant (p, T_u, Φ, EGR) conditions

3D-CFD METHODOLOGY

The 3D-CFD model of the engine was created using a customized version of SIEMENS PLM STAR-CD v4.30. The combustion chamber and both the intake and exhaust ports are included in the model. As shown in Fig. 3, symmetry is exploited to reduce the computational effort, given the use of a RANS modeling framework. As it will be furtherly outlined, this solution allows to counterbalance the very high computational cost introduced when adopting the soot sectional method model and a multicycle simulation approach. As already reported in the previous paragraph, the GDI optical unit under investigation features a non-negligible crevice volume which is included in the CFD model' to account for the blow-by losses. The total number of fluid cells ranges from 1.2 to 0.4 million cells at TDC and BDC, respectively. A detailed description of the CFD model can be found in [29,30] and the following details specifically focus on the modelling strategy adopted for the present study. All the calculations are carried out in the RANS framework using the k-ε RNG turbulence model for compressible flows. A dedicated 1D model of the engine was calibrated to derive time-varying pressure and temperature boundary conditions for both the intake and the exhaust port. An additional mass flow rate is applied at the annular area at the bottom of the crevice to model the blow-by losses. Uniform wall temperatures are applied at each engine component facing the combustion chamber and the GruMo-UniMore wall heat transfer model [31,32] is used to estimate wall heat transfer.

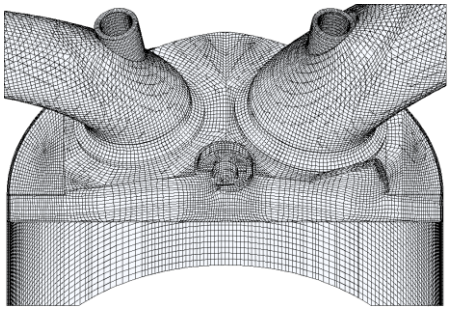

FIGURE 3. Detail of combustion chamber mesh

ECFM-3Z combustion model [33] customized with a methodology to accurately estimate laminar flame speed at engine-relevant conditions [28,34] is used. Since the study is focused on soot formation, which is the last of a long chain of in-cylinder processes, the highest possible degree of accuracy in describing the six-hole full-cone spray evolution and ensure a proper description of the equivalence ratio field at spark timing is required. Therefore, the spray is modelled following the approach described in [35] for multi-hole GDI injectors up to 60 MPa of injection pressure. While an accurate spray modelling approach is mandatory to predict spray penetration and spray plums pattern qualitatively determining the critical regions for liquid film formation, an additional modelling effort is required to quantitatively predict the spray-wall interaction and estimate the critical conditions leading to liquid film formation. For this reason, Senda droplet-wall interaction model [36] was used in conjunction with Habchi model [37] for Leidenfrost temperature determination. While previous investigations [38, 39] clearly showed that a multi-component approach is recommended to improve the prediction of pure and blended fuels' spray, a single component approach is here used to reduce the overall computational cost of engine simulations. Regarding soot emission modelling setup, the sectional method model was used with forty sections. This setup allows not only to have a higher degree of accuracy on PSDF, but also to cover the whole particle size range detected by the EEPS. This last point is crucial to properly model the PSDF since lower numbers of sections, e.g. 20 sections with a soot precursors' volume $V_{PAH} = 0.4 \cdot 10^{-27} m^3$, would yield a maximum diameter particle of diameter $d_{20,m} = 95\, nm$. In this way, a consistent comparison between experiments and simulation is guaranteed. As stated earlier, the soot model is used in conjunction with the constant pressure library whose details are reported in Table 3. In order to properly model soot formation and evolution during the combustion process, a multicycle simulation approach is adopted, for two main reasons. Firstly, no soot and soot precursors are present in the combustion chamber at combustion onset of the

first simulated cycle. This situation is obviously unrealistic as it leads to an underestimation of the main processes involved in soot formation and thus to an underestimation of PM, PN and PSDF. Moreover, since the model relies on a steady state assumption for soot precursors, an absence of soot mass fraction in the combustion chamber may lead to an underestimation of the condensation process in favor of a more pronounced nucleation process. In turn, this could lead to an overestimation of the number density of ultrafine particles. Secondly, the prediction of the soot source terms in a single CFD cycle is not representative of a cycle-averaged condition and it is affected by the adopted initial conditions. Local thermodynamic and mixture quality state convergence is an a-priori condition to properly evaluate the soot source terms. For the highlighted reasons, three consecutive cycles were performed in the present study to reach convergence on mixture distribution, liquid film deposits and combustion related quantities. When convergence was achieved, the sectional soot model was activated for three additional cycles to allow a correct development of the soot-related processes.

RESULTS

In this section, results from the six consecutive cycles are analyzed. For the sake of clarity, dark colors are used to represent the first three cycles while red is used for the last three ones. Such choice allows to distinguish the cycles carried out to reach convergence on the main fuel- and combustion-related quantities from those carried out to evaluate soot formation. In Fig. 4a-b-c, the evolution of liquid film formation on the piston, on the liner and on the dome is reported, respectively. In addition, the average equivalence ratio in the combustion chamber at spark timing, with and without crevices, is correlated with the evolution of liquid film mass on the piston crown at the start of combustion. As expected, most of the liquid film is formed on the piston crown due to the early injection strategy.

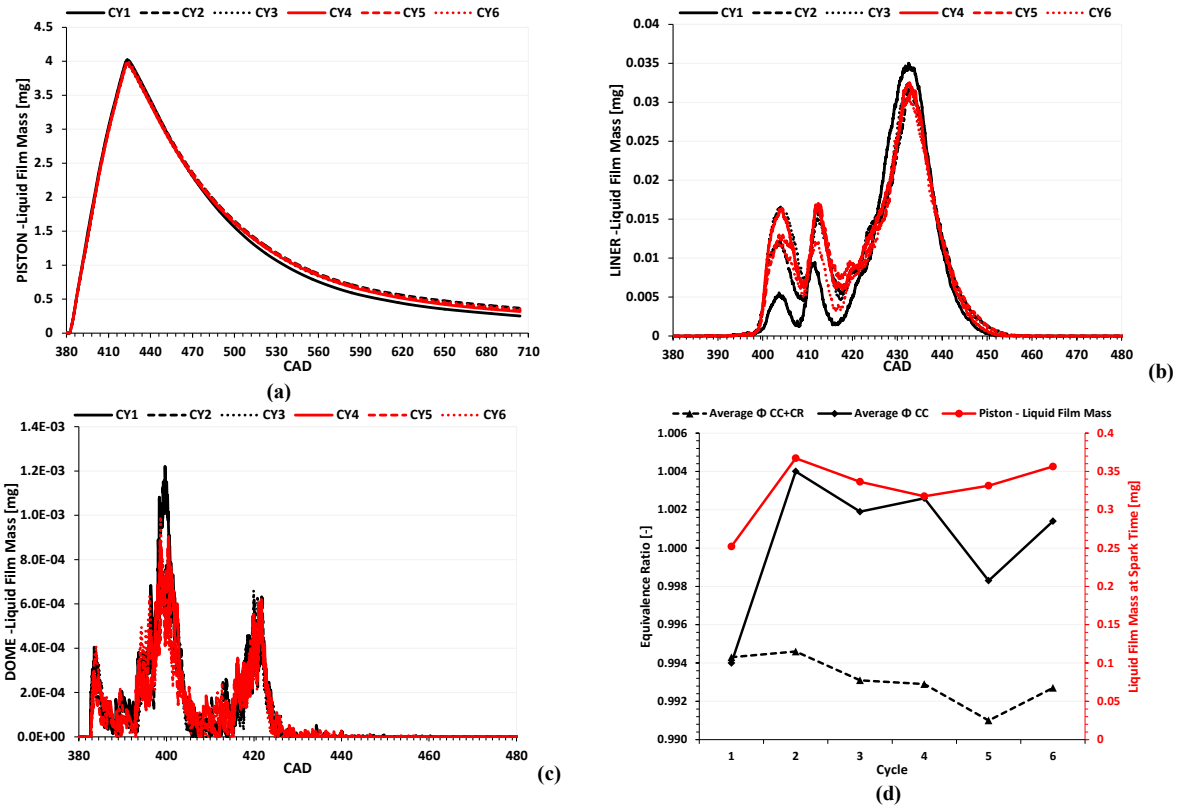

FIGURE 4. Liquid film mass on the piston crown **(a)**, on the liner **(b)** and on the dome **(c)** Average equivalence ratio in the combustion chamber (black solid line), in the combustion chamber plus the crevices (black dotted line), and liquid film mass on the piston crown (red solid line) **(d)**

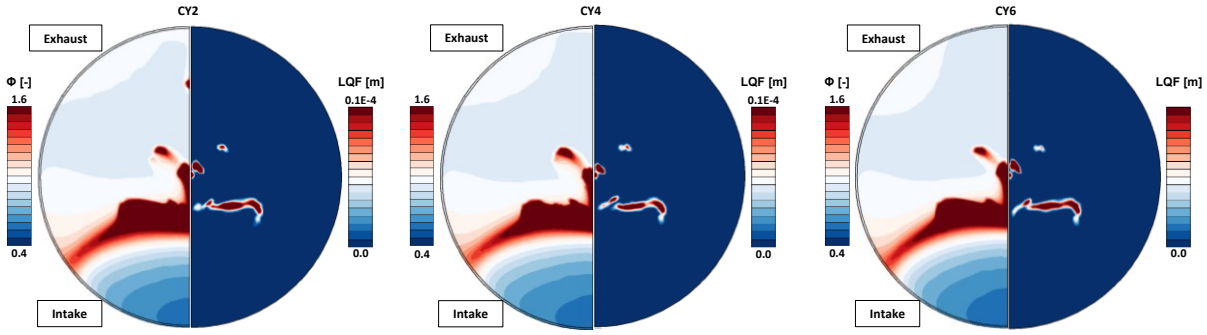

FIGURE 5. (a) Liquid film thickness pattern (right) and equivalence ratio field (left) on the piston crown over the engine cycles at spark timing.

In terms of spray evolution, the proximity of the piston to the dome during the injection process leads to a pronounced spray impingement on the former, which causes the formation of liquid film pools $(380\ CAD)$. Then the droplets rebound on the piston deviating in their trajectories and impacting on the dome $(385\ CAD)$ and the liner$(400\ CAD)$. It is noteworthy that the amount of liquid film formed on the piston is one and two orders of magnitude higher than the deposits formed on the liner and the dome, respectively. For this injection strategy, liquid film is a driving factor for soot formation since it persists at spark timing. Numerically speaking, the liquid film evolution on the piston crown and the average mixture equivalence ratio stabilize after the third engine cycle. A further confirmation is given by the liquid film pattern evolution on the piston crown at spark timing over the cycles, reported on the right in Fig. 5 for cycles 2, 4 and 6. The resulting equivalence ratio field on the piston crown is reported on the left side for the sake of completeness. It is possible to notice how the impingement pattern remains unchanged from the third cycle on. Similarly, the equivalence ratio distribution stabilizes and its average value in the combustion chamber reaches a value around 1.02. Liquid film pools are still present at spark timing on the piston crown in the central part of the chamber towards the intake side. Such impingement regions lead to the formation of local rich pockets, visible in Fig. 6. Comparing the evolution of mixture stratification over the cycles, it is confirmed that convergence is met after three cycles. A calibration of the combustion model is then performed to reproduce the experimental in-cylinder average pressure trace. To this aim, slight variations of the flame kernel imposed by the adopted ignition model are used. Such calibration brings to a variation of the flame kernel radius in the order of tenth of a millimeter. Once stratification and liquid film convergence is reached, no further calibration on the combustion model is needed for the following cycles.

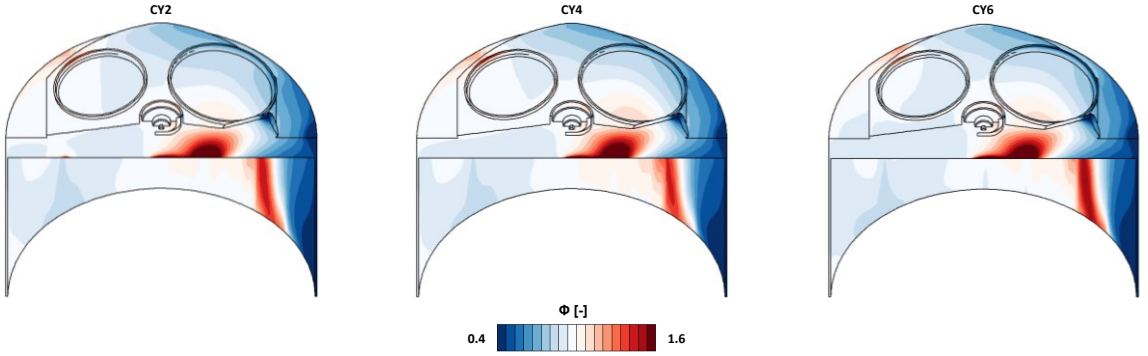

FIGURE 6. Equivalence ratio field over the engine cycles at spark timing.

A comparison between calculated and measured in-cylinder pressure traces is reported in Fig. 7a. Apparent heat release rate and its cumulative rate are reported in Fig. 7b and 7c respectively. A reasonable agreement is found. It is noteworthy that the first cycle exhibits a lower pressure peak because of the backflow of injected fuel mass in the intake port, which is then introduced at the following cycle during the scavenging process. This is responsible for the sudden increase of the equivalence ratio at the second simulated cycle, portrayed in Fig. 5d. As exhibited in Fig. 7a-7b, the heat release rate evolution over the cycle is well predicted by the model, although a slight overestimation of the apparent heat release rate is found for the peak pressure condition. This is due to a specific choice of the authors to accurately represent the early combustion phase (from 10% to 50% of mass fraction burnt) in order to give a precise estimation of the gas temperature increase, which is a key parameter influencing fuel pyrolysis and soot nucleation. As shown in Fig. 7a, this strategy leads to a good agreement of the simulated cycles with the experimental combustion indicators. The global combustion process duration, represented by the difference between MFB10 (10% of mass fraction burnt) and MFB90 (90% mass fraction burnt), is underestimated of 1.2 CAD.

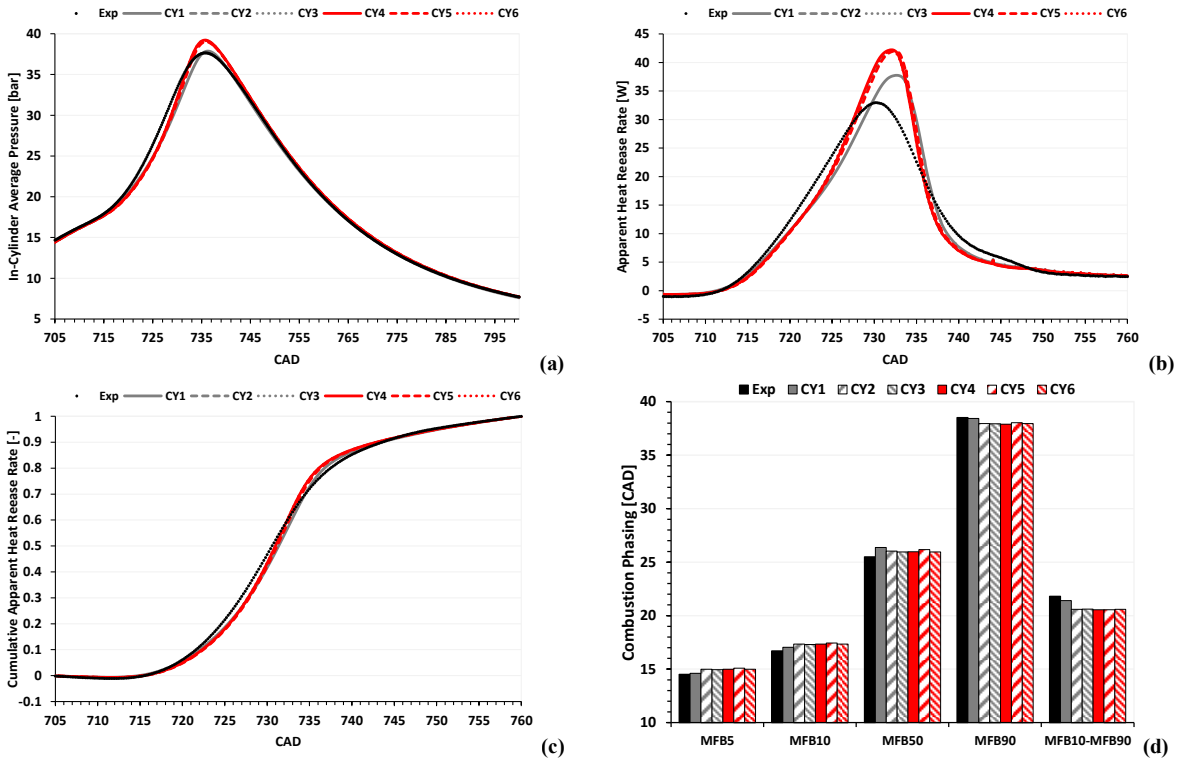

FIGURE 7. (a) Average In-Cylinder pressure traces: experimental (solid black line) vs calculated (solid colored lines) **(b)** Apparent heat release rate: experimental (solid black line) vs calculated (solid colored lines) **(c)** Cumulative apparent heat release rate: experimental (solid black line) vs calculated (solid colored lines) **(d)** Combustion indicators, phasing and duration: experimental (solid black bar) vs calculated (colored bars).

A visual representation of the combustion process development is reported in Fig. 8, for the sixth simulated cycle for selected CADs. Soot mass iso-surface portraying cells with a soot mass ranging from 0.1e-5 mg to 0.1e-3 mg is reported. Focusing on the early stages of combustion, at +5 CAD after Start of Combustion (aSOS), soot is already present in the combustion chamber, under the exhaust valve, due to the incomplete discharge of exhaust gases during the scavenging processes. At +25 CAD aSOS the flame front is approaching the end-gas region where the soot mass inherited by the previous cycle is oxidized while soot mass is formed in the local rich spot present in between the piston and the intake valve. As combustion evolves the liquid film pools, present on the piston crown at spark timing slowly evaporates and it burns during the late stages of combustion. As portrayed at +75 CAD aSOS, a separate soot mass pocket is formed in the central part of the combustion chamber from the liquid film pools previously analyzed in Fig. 5. While the soot formation processes are dominant in the first part of the combustion process, the oxidation source terms dominate in the late combustion stages, as shown by the individual average source terms over the cycle, reported in Fig.9. It must be noted that the overall coagulation source term is not reported since it is always null by definition. Conversely, the surface growth source term is reported being non-null, although of one order of magnitude lower compared to the other sources. This last result is in line with results obtained by previous application of the model to engine applications [20]. As suggested in previous studies [16,18,20], soot quantities are quantitatively evaluated at Exhaust Valve Opening (EVO), since it would be computationally too demanding to include the entire exhaust manifold in the simulated domain. In the experiments, exhaust gases are sampled in the exhaust line and analyzed by the EEPS which provides PM, PN, and PSDF measurements in terms of concentration. For this reason, the calculated soot quantities are expressed to the sampling reference thermodynamic conditions in the EEPS ($p_{EEPS} \approx 1\ bar, T_{EEPS} = 323\ K$). The dilution rate used in the experiments is also accounted for when calculating the calculated soot quantities concentration referring to the EEPS sampling conditions. In Fig. 10a, both the overall and ultrafine soot mass concentrations measured at the exhaust are compared to the CFD results of the last three cycles. In order to compare the calculated data with the experimental ones consistently, the overall soot mass concentration was calculated considering only the sections whose mean diameter was included in the sampling diameter range of the instrument ($5\ nm \leq d \leq 560\ nm$). Similarly, only the sections whose mean diameter was included in the 30 nm $\leq$ d $\leq$ 50 nm range were considered to calculate the overall ultrafine soot mass concentration. The same rationale was used to calculate the overall and ultrafine soot number concentrations, reported in Fig. 10b. It must be kept in mind that $+100\%/-50\%$ is a common target used by

the engine manufacturers in the field of engine soot modelling when evaluating PM [20]. Similarly, PN is commonly considered satisfactorily predicted when within one order of magnitude of the experimental data [17].

Observing the evolution of the soot quantities evaluated at EVO over the cycles, a marked gap is present between the first and the following cycles. This confirms that at least two engine cycles must be simulated when performing soot calculations for GDI powered units. If the criterion for particle number density is used to compare experimental and calculated data, all the results are well within one order of magnitude for all the three cycles performed, although the best result overall is obtained with the first one. This is due to the overestimation of the soot particle number for the small particles, which accumulate over the cycles instead of being consumed. Under a pure modelling standpoint, this overestimation could be caused by the constant soot density assumption of the sectional method, which neglects the difference of collision frequency factor of particles of different sizes [18]. If the total soot mass concentration is considered, it is possible to notice how more than a single soot cycle is needed to properly estimate the total soot mass. In particular, a very good agreement is obtained in terms of total soot mass with a second soot cycle. The estimated overall soot mass concentration is 240 mg/m^3 against the 206 mg/m^3 measured one. Therefore, the relative error exhibited by the 3D CFD model is only +16.5%. It is noteworthy that performing a third soot cycle does not affect the results and that convergence is met, in terms of soot characteristic quantities, within three soot cycles. The overall soot mass concentration overestimation is due to a non-negligible overestimation of the ultrafine soot mass concentration.

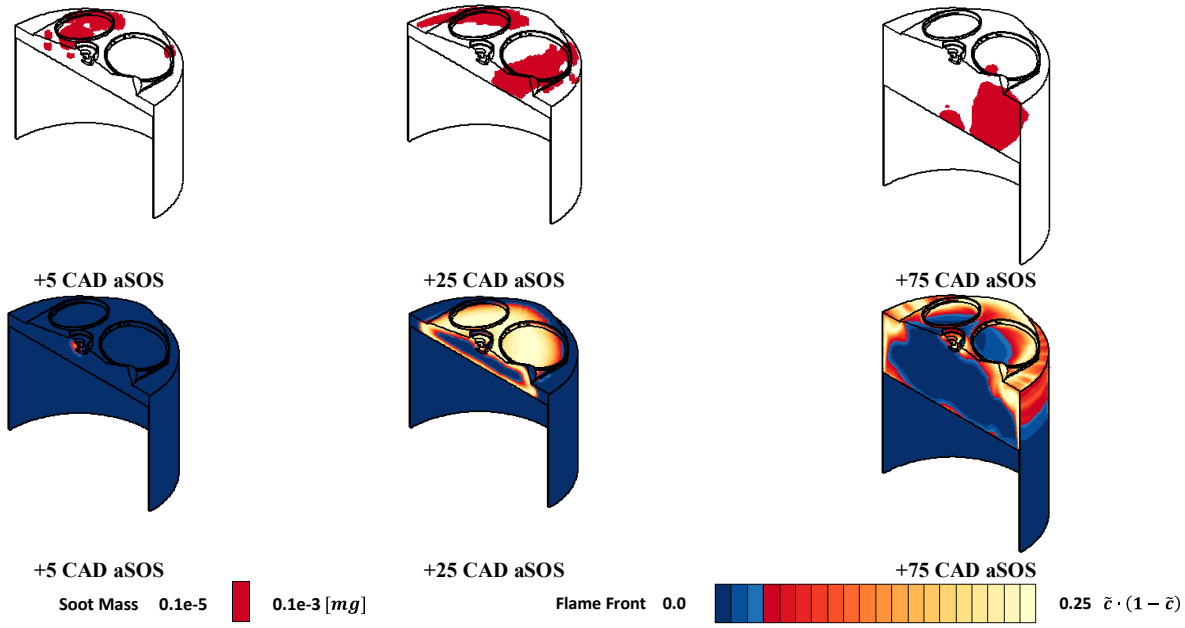

FIGURE 8. soot formation at key CAD during the sixth engine cycle. Soot iso-surface in red, contour plots of flame front based on the local progress variable value

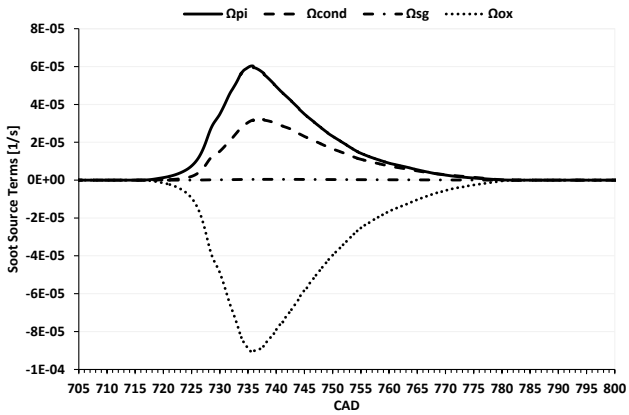

FIGURE 9. Nucleation (Ωpi), condensation (Ωcond), surface growth (Ωsg) and oxidation (Ωox) average source terms in the combustion chamber.

Considering the second soot cycle's results, the 3D-CFD model predicts an ultrafine soot mass concentration of 1.60 mg/m^3 against the 0.85 mg/m^3 measured one, which corresponds to a +88.2% relative error. While further

improvements under the soot modelling point of view might reduce the errors on the estimated soot quantities, this results clearly demonstrate that being able to match the experimental PSDF is fundamental to precisely quantify PM and PN, as shown in Fig. 10c-10d. A multicycle approach is mandatory to properly estimate all the processes involved in soot formation. Furthermore, convergence over the cycles of soot related quantities is necessary to quantitatively estimate the average diameter of the soot particles population produced. Despite the ultrafine soot particle density issue, the error is within one order of magnitude. Several experimental studies [40-42] have shown that the effective particle density is maximum for the primary particles and it decreases exponentially with the mobility diameter. As a final remark, this overestimation has an effect in terms of quantitative results especially if the arithmetic average diameter of the distribution is calculated, resulting in an underestimation compared to the experimental value. In practical terms, a very good agreement with the experiment is found if the local maximum of the 3D CFD PSDF around 100 *nm* is considered as representative of the engine-out soot particles average diameter.

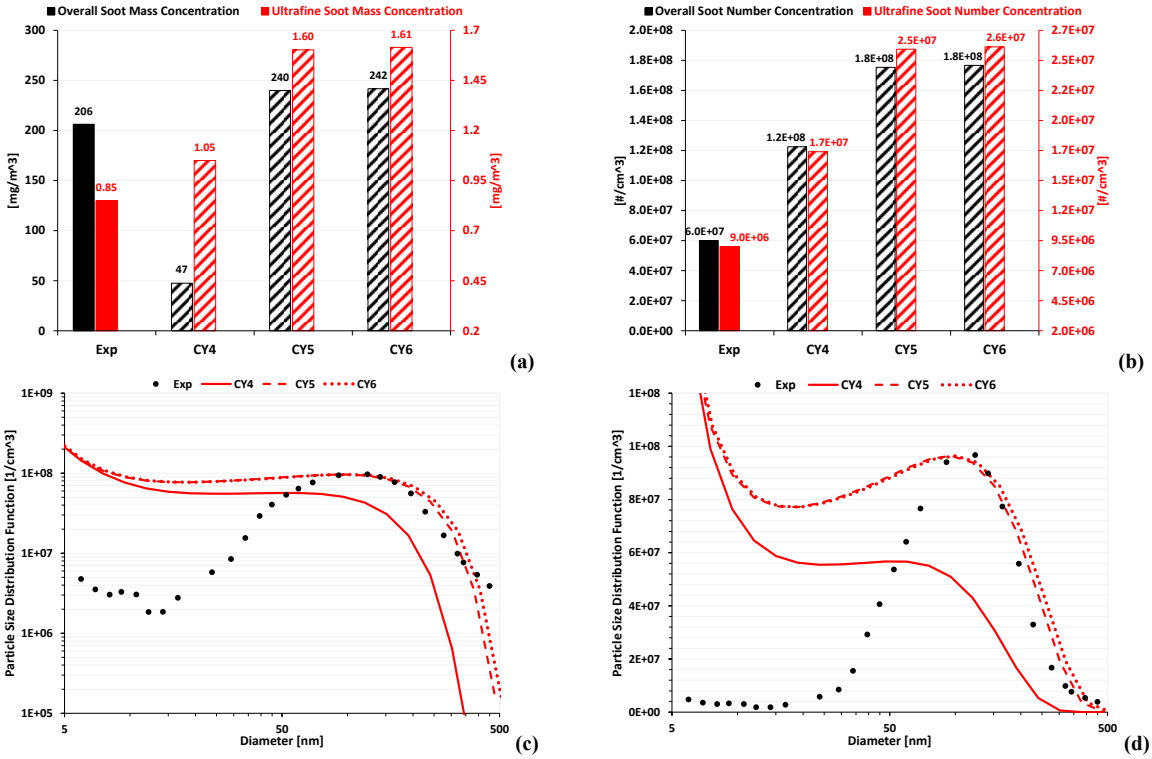

FIGURE 10. (a) (b) Overall and ultrafine soot mass and number concentrations. Solid bars: experimental data; striped bars: CFD results **(c), (d)** Experimental and calculated PSDF on a logarithmic and on a linear scale. Experimental data: filled black dots; calculated data: red lines

CONCLUSIONS

A customized version of the sectional method soot model was used to predict PM, PN and PSDF soot emissions measured on an optically accessible GDI unit. A single operating point, characterized by an early injection strategy, was chosen to demonstrate that the model can be used to quantitatively predict GDI soot emissions. A modified PAH mechanism was proposed and validated against premixed flat flame burner experiments. It was then used to generate dedicated soot libraries for the engine case considered via 0D constant pressure simulations. A 3D-CFD model [43] of the investigated research engine was used to perform multicycle combustion and soot numerical simulations; a preliminary detailed analysis of the spray and liquid film formation was carried out, due to its relevance for the subsequent soot analysis. The final results demonstrate that using the proposed methodology it is possible to quantitatively predict PM, PN and especially the PSDF. It is shown that if enough engine cycles are performed, the accumulation mode becomes dominant and convergence, in terms of characteristic soot quantities, is reached. Due to the intrinsic assumption of the sectional method model, the accumulation of lower diameter particles leads to an overestimation of the soot number concentration and a slight overestimation of the soot mass concentration, since these are modelled as spherical particles with the same density as the smaller ones, in contrast with experimental evidences of decreasing density with particle size. Further investigations will be carried out to further validate the approach on other operating points and to account for variable particle density as a function of the diameter.

ACKNOWLEDGEMENTS

The experimental soot measurements were carried out by Dr. Silvana Di Iorio at the Istituto Motori of the National Research Council of Italy (IM-CNR), who is gratefully acknowledged.

REFERENCES

1. *P. Thunis et al. "Urban PM2.5 Atlas – Air Quality in European cities". EUR 28804 EN, doi:10.2760/336669, JRC108595*
2. *"IARC: Diesel Engine Exhaust Carcinogenic". International Agency for Research on Cancer (WHO), Press Release n.213, June 2012.*
3. *N.A.H. Janssen et al. "Health effects of Black Carbon". WHO – Regional Office for Europe, ISBN: 978 92 890 0265 3.*
4. *H. Fuchsig et al. "World Medical Association's Concern Regarding Effects of Ultrafine Particles and Vehicular Emissions: Report from 65th General Assembly in Durban- South Africa". Emiss. Control Sci. Technol. (2017) 3:243-244 (2017)*
5. *C.L. Myung et al. "Exhaust nanoparticle emissions from internal combustion engines: a review". Int. J. Automot. Technol. 2012;13(1):9-22. 10.1007/s12239-012-0002-y.*
6. *V. Knop et al. "Comparison of PFI and DI Operation in a Downsized Gasoline Engine". (2013). SAE International Journal of Engines. 6. 941-952. 10.4271/2013-01-1103.*
7. *H. Fu et al. "Impacts of Cold-Start and Gasoline RON on Particulate Emission from Vehicles Powered by GDI and PFI Engines". (2014). SAE Technical Papers. 2014. 10.4271/2014-01-2836.*
8. *M. Raza et al. "A Review of Particulate Number (PN) Emissions from Gasoline Direct Injection (GDI) Engines and Their Control Techniques". (2018) Energies. 6. 10.3390/en11061417.*
9. *X. He et al. "Effects of Gasoline Direct Injection Engine Operating Parameters on Particle Number Emissions". (2012). Energy & Fuels - ENERG FUEL. 26. 2014-2027. 10.1021/ef201917p.*
10. *A. Irimescu et al. (2018). "Investigation on the effects of butanol and ethanol fueling on combustion and PM emissions in an optically accessible DISI engine". Fuel. (2018) 216. 121-141. 10.1016/j.fuel.2017.11.116.*
11. *A. Überall et al. "A literature research about particle emissions from engines with direct gasoline injection and the potential to reduce these emissions". Fuel, Volume 147, 2015, Pages 203-207, ISSN 0016-2361, https://doi.org/10.1016/j.fuel.2015.01.012.*
12. *J. Qi et al. "The Effect of Operating Parameters on Soot Emissions in GDI Engines". SAE International Journal of Engines, vol. 8, no. 3, 2015, pp. 1322–1333.*
13. *K. Netzell et al. "Calculating the soot particle size distribution function in turbulent diffusion flames using a sectional method". Proceedings of the Combustion Institute, Volume 31, Issue 1, 2007, Pages 667-674, ISSN 1540-7489, https://doi.org/10.1016/j.proci.2006.08.081.*
14. *K. Netzell, "Development and Application of Detailed Kinetic Models for the Soot Particle Size Distribution Function", PhD Thesis, Lund Institute of Technology, 2006.*
15. *F. Mauss et al. "Particle Size Distribution Functions in Laminar and Turbulent Flames". (2019)*
16. *C. Marchal, "Modélisation de la formation et de l'oxydation des suies dans un moteur automobile". Université d'Orleans, 2008. https://tel.archives-ouvertes.fr/tel-00392316.*
17. *D. Aubagnac-Karkar, "Modélisation des suies par méthode sectionnelle pour la simulation RANS des moteurs Diesel". Mécanique des fluides. Ecole Centrale Paris, 2014. https://tel.archives-ouvertes.fr/tel-01132323.*
18. *C. Marchal et al. "Soot modelling in automotive engines". Proc. of the European Combustion Meeting, 2009*
19. *P. Vervisch-Kljakic, "Modèlisation des oxydes d'azote et de suies dans les moteurs Diesel". Ph.D. Thesis, Ecole Centrale Paris, 2011.*
20. *D. Aubagnac-Karkar et al. "Sectional soot model coupled to tabulated chemistry for Diesel RANS simulations", Combustion and Flame, Volume 162, Issue 8, 2015, Pages 3081-3099, ISSN 0010-2180, https://doi.org/10.1016/j.combustflame.2015.03.005.*
21. *F. Bonatesta et al. "Combustion and Particulated Matter Formation in Modern GDI Engines: A Modelling Study Using CFD". F2016-ESYG-018.*
22. *I. Glassman, "Soot formation in combustion processes". Symposium (International) on Combustion, Volume 22, Issue 1, 1989, Pages 295-311, ISSN 0082-0784, https://doi.org/10.1016/S0082-0784(89)80036-0.*
23. *Y. An et al. "Development of a PAH formation model for gasoline surrogates and its application for GDI engine CFD simulation". Energy,Volume 94,2016,Pages 367-379, ISSN 0360-5442,https://doi.org/10.1016/j.energy.2015.11.014.*

24. *F. Inal et al. "Effects of equivalence ratio on species and soot concentrations in premixed N-heptane flames". (2002). Combustion and Flame. 131. 16-28. 10.1016/S0010-2180(02)00388-7.*
25. *G. Blanquart et al. "Chemical mechanism for high temperature combustion of engine relevant fuels with emphasis on soot precursors". Combustion and Flame, Volume 156, Issue 3, 2009, Pages 588-607, ISSN 0010-2180, https://doi.org/10.1016/j.combustflame.2008.12.007.*
26. *A.T. Hartlieb et al. Combust. Flame 121 (2000) 610-624.*
27. *A. Tregrossi et al. Combust. Flame 117 (1999) 553-561.*
28. *M. Del Pecchia et al. "Development of Chemistry-Based Laminar Flame Speed Correlation for Part-Load SI Conditions and Validation in a GDI Research Engine". (2018) SAE International Journal of Engines. doi:10.4271/2018-01-0174.*
29. *S. Breda et al. "Numerical Simulation of Gasoline and n-Butanol Combustion in an Optically Accessible Research Engine". SAE Int. J. Fuels Lubr. 10(1):2017, doi:10.4271/2017-01-0546.*
30. *S. Breda et al. "CFD Analysis of Combustion and Knock in an Optically Accessible GDI Engine". SAE International. Journal of Engines 9(1):641-656,2016,doi:10.4271/2016-01-0601.*
31. *G. Cicalese et al. "Integrated In-Cylinder / CHT Methodology for the Simulation of the Engine Thermal Field. An Application to High Performance Turbocharged DISI Engines" SAE Int. J. Engines 9(1):601-617, 2016, doi:10.4271/2016-01-0578.*
32. *F. Berni et al. "A modified thermal wall function for the estimation of gas-to-wall heat fluxes in CFD in-cylinder simulations of high performance spark-ignition engines". Applied Thermal Engineering, 115, pp. 1045-1062, 2017. DOI: 10.1016/j.applthermaleng.2017.01.055*
33. *O. Colin et al. "The 3-Zone Extended Coherent Flame Model (ECFM-3Z) for computing premixed/diffusion combustion". (2004) Oil Gas Sci. Technol. – Rev. IFP 59, 6, 593-609.*
34. *A. d'Adamo et al. "Chemistry-Based Laminar Flame Speed Correlations for a Wide Range of Engine Conditions for Iso-Octane, n-Heptane, Toluene and Gasoline Surrogate Fuels", SAE Technical Paper 2017-01-2190, 2017.*
35. *L. Postrioti et al. "Experimental and Numerical Analysis of Spray Evolution, Hydraulics and Atomization for a 60MPa Injection Pressure GDI System". SAE Technical Paper 2018-01-0271, 2018,https://doi.org/10.4271/2018-01-0271.*
36. *C. Lee et al. (2001) "A Study on the Spray-Wall Interaction Model considering Degree of Superheat in the Wall Surface". (2001). Numerical Heat Transfer, Part B: Fundamentals, 40:6,495-513,doi:10.1080/104077901753306610.*
37. *C. Habchi, "A Comprehensive Model for Liquid Film Boiling in Internal Combustion Engines", Oil & Gas Science & Technology – Rev. IFP, 65(2), pp. 847-949.*
38. *S. Malaguti et al. "Experimental and Numerical Characterization of Gasoline-Ethanol Blends from a GDI Multi-Hole Injector by Means of Multi-Component Approach". SAE Technical Paper 2013-24-0002, 2013, https://doi.org/10.4271/2013-24-0002.*
39. *N. Giovannoni et al. "CFD Analysis of the Effects of Fuel Composition and Injection Strategy on Mixture Preparation and Fuel Deposit Formation in a GDI Engine". SAE Technical Paper 2015-24-2408, 2015, https://doi.org/10.4271/2015-24-2408.*
40. *M. Matti Maricq et al. "The effective density and fractal dimension of soot particles from premixed flames and motor vehicle exhaust". J. Aerosol Science, 35:1251-1274.*
41. *K. Park et al. "Relationship between Particle Mass and Mobility for Diesel Exhaust Particles". (2003). Environ. Sci. Technol. 37:577-583.*
42. *J. Xue et al. "Using a new inversion matrix for a fast-sizing spectrometer and a photo-acoustic instrument to determine suspended particulate mass over a transient cycle for light-duty vehicles". Aeros. Sci. Tech., (11), 1227-1238.*
43. *S. Fontanesi et al. "A methodology to improve knock tendency prediction in high performance engines". Energy Procedia, 45, pp. 769-778, 2014. DOI: 10.1016/j.egypro.2014.01.082*